Proceedings of CHT-04
ICHMT International Symposium on Advances in Computational Heat Transfer

April 19-24, 2004, Norway

CHT-04-179

VERIFICATION AND VALIDATION OF *EFD.Lab* CODE FOR PREDICTING HEAT AND FLUID FLOW

V. Balakin[*°], A. Churbanov[*,**], V. Gavriliouk[*], M. Makarov [*]and A. Pavlov[*]
[*]NIKA Software, 4 Volokolamskoye Shosse, 125993 Moscow, Russia
[**]Institute for Mathematical Modeling, 4-A Miusskaya Sq., 125047 Moscow, Russia
[°]Correspondence author: Fax: +7 (095) 785-5748 Email: balakin@nika.sokol.ru

ABSTRACT Results of verification and validation of commercial code EFD.Lab are presented in this paper. Two classes of tests – so-called fundamental as well as applied industrial – are considered for heat and fluid flow phenomena. A flow over a circular cylinder with internal heating and buoyancy-driven flow in a square cavity have been predicted among fundamental tests in a wide range of governing parameters. Another examples that demonstrate accuracy and efficiency of EFD.Lab to solve applied problems of practical interest are concerned with electronic cooling. Pin-fin and plain configurations of heat sinks have been predicted in the free and forced convection regimes, respectively, taking into account radiation effects. Grid convergence studies have been performed during validation predictions. A good agreement has been obtained between numerical and experimental data in all predicted tests in a wide range of computational grids.

INTRODUCTION

This work is concerned with verification and validation (V&V) of the commercial code – EFD.Lab (Engineering Fluid Dynamics Laboratory), a product of NIKA GmbH (www.nika.biz) - a general-purpose CFD code that belongs to a new generation of codes based on recent achievements in user-friendly interface as well as highly accurate, robust and automatic numerics.

The basic concept put into the background of designing EFD.Lab is to maximize as high as possible automatization level in preparing, performing and visualizing predictions of real applied engineering problems. This tendency to make CFD tools less expensive as well as easier and closer to engineers only recently has been "discovered" and taken to implementation in The Big Three of CFD - Fluent, CFX (recently purchased by ANSYS Inc.), and STAR-CD (CD adapco Group) [1].

In comparison with traditional CFD codes oriented to high-level specialists in CFD (Ph.D. as the rule), EFD.Lab is designed for a wider category of users – engineers of different special interest. In their daily activities they occasionally face the necessity to solve complex industrial problems coupled with heat and fluid flow phenomena. To accomplish these ends, EFD.Lab has some specific features, namely: complete integration with CAD-systems; totally automatic grid generation; automatic prescribing of computation control parameters; user-friendly pre- and post-processing; a possibility to perform a parametrical study of a problem *etc*. The code does not require tuning a somewhat mystique parameters of the algorithm or choosing one of several not very clear models or approximations. These combined possibilities allow accelerating essentially

solution of day duty problems for an engineer but imposing high requirements on accuracy and reliability of such an automatic approach. That is why during its development EFD.Lab has been exposed to the detailed verification and validation (V&V) procedure on a host of analytical and benchmark solutions as well as on experimental results available from publications and databases [2,3]. Some of the results are discussed in the present work with particular emphasis on the heat transfer phenomenon.

EFD.Lab: MODELS, MESHES, NUMERICS AND LINEAR SOLVER

Below there are briefly listed features of EFD.Lab.

Models The employed in the code numerical method is designed for laminar and turbulent flows ranging from incompressible to highly compressible flows. Heat transfer simulation includes forced, natural and mixed convection, conjugate heat transfer in solids and liquids, radiation *etc*.

The approach is based on the Reynolds-Averaged Navier-Stokes equations. The energy conservation equation for the total enthalpy in a fluid and temperature in a solid media along with a specially designed model of energy exchange on a solid-liquid interface are used to govern heat transfer.

Sub-grid flow field peculiarities such as vortices and boundary layers are resolved using the following integral techniques: modified (k-ε)-turbulence model describing laminar, mixed laminar/turbulent and turbulent regimes coupled with an original near-wall laminar/turbulent model.

Meshes The code essentially exploits adaptive mesh refinement strategy [4,5] that provides an automatic adaptation of a Cartesian computational grid to the complicated geometry of a computational domain (static adaptation) and to the solution peculiarities (dynamic adaptation). This allows combining merits of employing high order spatial approximations and local resolution of solution or geometry singularities without essentially increasing the number of cells. Grid cells are treated as control volumes and can belong completely to a fluid or solid, or contain both media. In the last case two phases are separated by a surface where heat and fluid flow should be considered in a specific way.

Numerics The finite volume method is utilized to derive conservative discrete equations [6-9]. All calculated unknowns are referred to cell mass centers, i.e. the collocated grid is used. The momentum components, pressure and total enthalpy are considered as the primary variables.

An operator-splitting technique similar to SIMPLE-type methods (so-called pressure-correction methods) in the time-dependent formulation is used to resolve the pressure-velocity coupling. Following the approach, firstly, the continuity and momentum equations are discretized, and then the discrete pressure correction equation is derived by means of algebraic transformations of the original grid equations with incorporated boundary conditions for momentum [10]. Usage of specially designed consistent approximations for operators of divergence in the continuity equation and gradient in the momentum equation leads to a linear system with the matrix that is close to symmetric positive definite one.

Second order approximations are used for all spatial operators, including convective terms. To provide monotonic solutions, non-linear flux approximations with limiters (like in the TVD approach) are employed for convective terms. Considering heat transfer problems, a single algebraic system is derived for solid and fluid media (the conjugate formulation of a thermal problem).

Multigrid solver Grid equations arising from discretization and linearization of the governing PDEs are solved using multigrid technique [11,12], thus obtaining near linear performance in terms of computational effort, as the mesh finesse increases.

Building the series of coarse meshes and appropriate linear system matrices is fully automatic and independent of the way the computational mesh is constructed. The Galerkin operators are used on the coarse grids. This ensures high (fine mesh cell number)/(coarse mesh cell number) ratio. No discretization on the sequence of coarse meshes is needed.

Automatic coarse grid construction takes full advantage of structured locally refined rectangular hexahedral mesh. To speed up the coarse grid construction, binary tree-like ordering of mesh cells is introduced. This facilitates addressing mother cell and neighbor cells in the construction process. Once a coarse mesh is built, block technique is used, that allows associating a pack of unknowns with any cell of any mesh (background computational or any coarse one). This feature improves performance in cases with complex geometry of computational domain. Since the domain geometry cannot be resolved on coarse grids, treads of unknowns are automatically tracked through the coarsening process, so that the pack in any cell is formed by representatives of different treads. Treads vanish as their representatives become involved in linear equations on coarse grids with other tread representatives.

The same technique is exploited when more than one unknown of the original linear system is associated with a cell of the mesh. Solving for temperature in the conjugated heat transfer model can be an example. On a subset of mesh cells, both fluid temperature and solid body temperature are components of the coupled system that is solved using multigrid technique sharing the same set of coarse grids.

As smoothers, Gauss-Seidel type relaxation methods are used, which are enhanced, if necessary, by introducing point-wise local iterative parameter. The choice of the parameter is sensitive to the genuine differential equation and the way it is approximated.

VERIFICATION AND VALIDATION METHODOLOGY

There do exist a good many approaches to V&V-procedure analyzed, e.g., in [13-15]. In our practice we employ for V&V procedure the benchmark results that, in our mind, can be decomposed into two classes – the so-called fundamental tests and applied industrial ones. Each of these classes has its own merits and demerits, but these two types complement each other nicely and are used successfully for the V&V-procedure of EFD.Lab. Let us consider these two classes for thermal problems.

The first class is the fundamental tests which are simple enough in sense of geometry (2D as the rule) and problem formulation (reduced models, exact boundary conditions *etc*.). On these low cost tests it is possible to conduct a parametrical study of various regimes of heat and fluid flow in a maximally wide range investigated experimentally, numerically or analytically. Moreover, versatility of fundamental tests allows investigate practically on the same configuration various physical effects in coupled or decoupled manner or even in artificial formulation in order to highlight their specific impact.

The second one – applied industrial problems where in addition to the complicated 3D geometry a combination of different strongly coupled physical phenomena takes place. Moreover, the exact values of material properties as well as operating conditions for device components are necessary in this case and so, the level of uncertainty is here much higher.

The automatic settings of the code input parameters are used in V&V-procedure calculations: the totally automatic grid generation, settings for control and calculation parameters as well as for stopping criteria are taken by default and so on. It is also possible to construct grids in a non-automatic way – uniform or stretching grids in accordance with input parameters specified by a user. Such simple grids are used for predictions or convergence studies in rectangular/parallelepiped computational domains.

The grid convergence is studied thoroughly for all tests: a series of calculations is carried out at different Result Resolution Level (RRL) – an input parameter for the code ranging from 1 up to 8 and increasing grid adaptation (and as the consequence its size) as well as convergence criteria. In fact, it is an integral parameter prescribing accuracy of predictions. The value of RRL that indicates no essential variation in computational results at its further increasing is treated as the final one and is recommended for a user.

FUNDAMENTAL TESTS

Flow over a circular cylinder with heating A flow over a circular cylinder is a remarkable test due to a host of data available for a comparison [16-19] where results of many researches are accumulated. Very useful guide [18,19] should be highlighted because there are condensed practically all experimental and numerical results derived for many years. Even in the 2D formulation this problem allows to investigate various regimes - steady-state and periodically oscillating, laminar and turbulent, and moreover, to study influence of such physical effects as compressibility, heat transfer, surface roughness, cylinder oscillation, cavitation, rheology (non-newtonian fluids) *etc.*

The simplest modification of this problem in order to involve heat transfer phenomenon is to consider a cylinder heated by the uniformly distributed in it a volumetric heat source with the total heat generation rate q [20]. Convective heat transfer from a heated circular cylinder in an air flow was studied numerically via EFD.Lab at Reynolds number Re_D from 1 up to 10^5, i.e. there were investigated flow regimes from steady-state up to developed transient flows with separation of laminar or turbulent boundary layer and as the consequence, various conditions of heat transfer were under the consideration.

The results of the grid convergence study for this problem are presented in Fig. 1 for $Re = 10^4$ as the dependence of predicted Nusselt number Nu_D on the value of RRL parameter. Here $Nu_D = h\,D/k$ (h is the heat transfer coefficient averaged over the cylinder, and k - fluid thermal conductivity), and the Prandtl number $Pr = 0.72$ for all values of Re_D. Evidently, EFD.Lab predictions lie within bounds of experimental data which have a large dispersion in this turbulent flow regime.

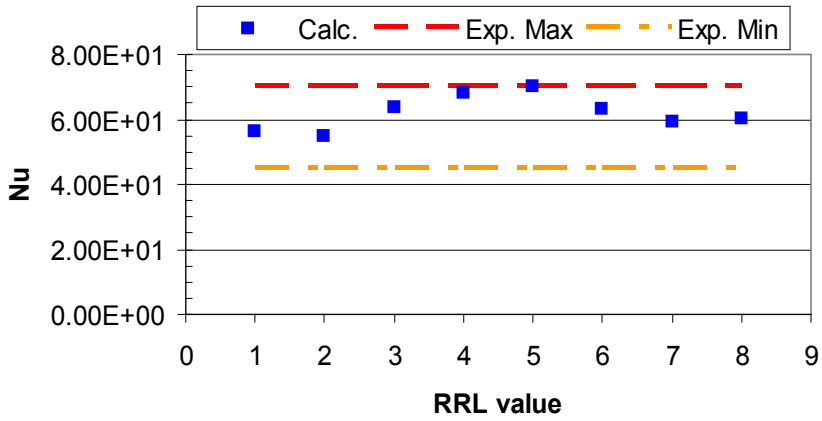

Figure 1. Grid convergence study: Nusselt number Nu_D vs. RRL value in comparison with experimental data from [20], $Re = 10^4$.

A good correlation in Nu_D between transient computations and measurements [20] has been obtained in the whole considered range of Re_D (see Fig. 2).

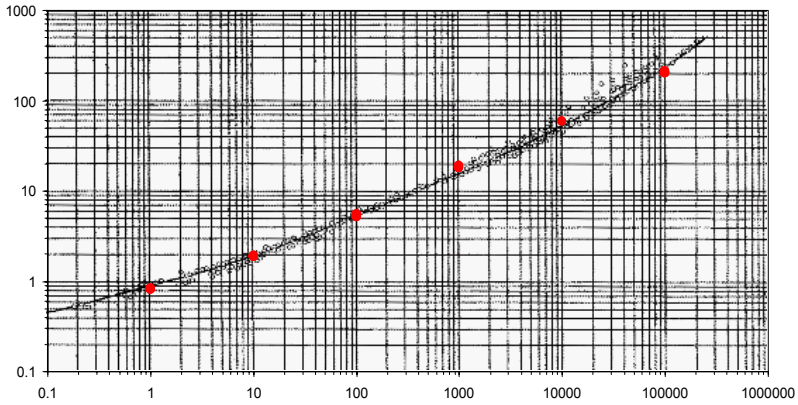

Figure 2. Nusselt number Nu_D for air flow over a heated cylinder: EFD.Lab predictions (red dots) in comparison with experimental data from [20] (black circles).

Buoyancy-driven cavity flow The well-known problem of a buoyancy-driven flow in a square cavity [21] has been considered, too. This 2D test is classical for convective heat transfer and allows to evaluate calculations quality in a simple geometry for the Rayleigh number varying from 10^3 up to 10^6. The benchmark solution [21] has been obtained from high-accurate predictions of about 40 computer codes and moreover, it agrees very well with the semi-empirical formula of experimental researches [22]. Nowadays this problem becomes a popular 3D test for various commercial and in-house codes [23]. In this 2D test a free convection is considered in a square cavity with isothermal side walls of different temperature value and the thermally insulated top and bottom. Air with variable properties has been used in EFD.Lab predictions of this problem.

A grid convergence study for the whole range of the Rayleigh number is presented in Fig. 3. This figure demonstrates dependence of ratio $Nu/Nu_{benchmark}$ both on the RRL value and on cell number per reference L (square cavity size). Such a norm of comparing is taken due to the fact that adaptive grids are employed in 2D EFD.Lab predictions and so, this presentation allows make a comparison with standard uniform or stretching grids. This plot confirms grid convergence achieved at RRL = 8. Numerical results derived at this value of RRL are shown below.

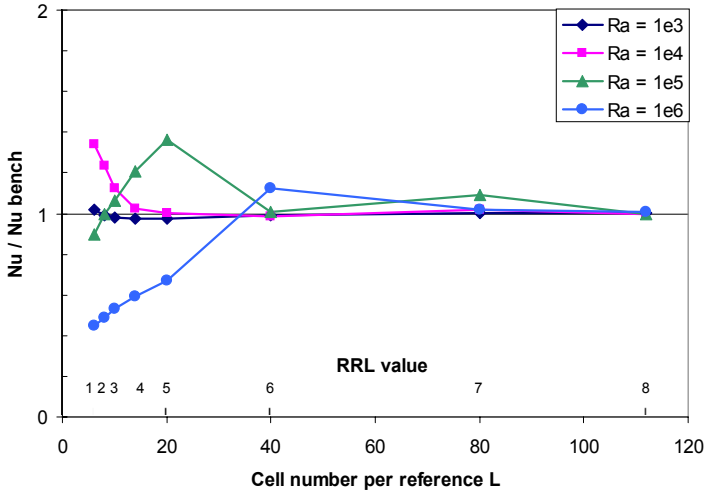

Figure 3. Grid convergence study: ratio $Nu/Nu_{benchmark}$ for various Ra.

Figure 4 shows the particular case of $Ra = 10^6$, predicted at the highest RRL = 8. The mesh derived in this prediction after the dynamic adaptation to the solution peculiarities is shown in Fig. 5. It is easy to see that this mesh matches well the features of heat and fluid flow.

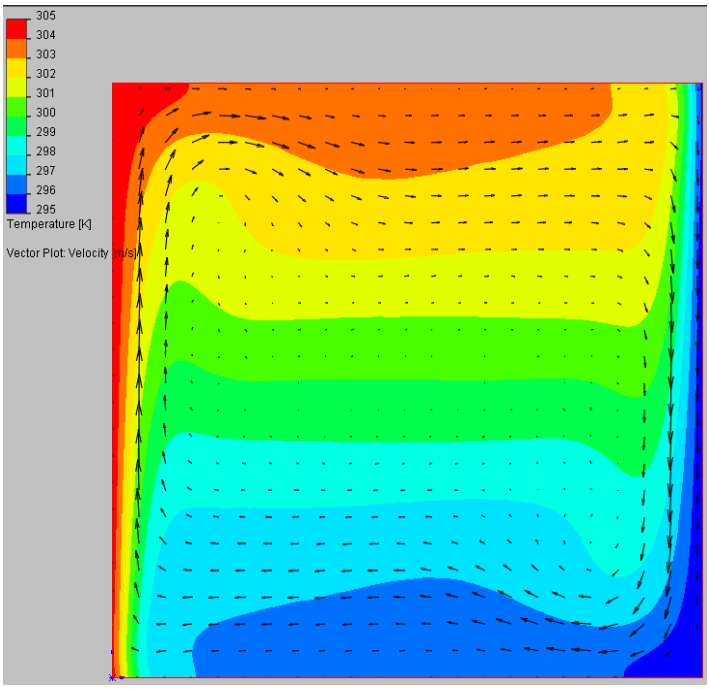

Figure 4. Temperature and velocity fields, predicted at RRL = 8 for $Ra = 10^6$.

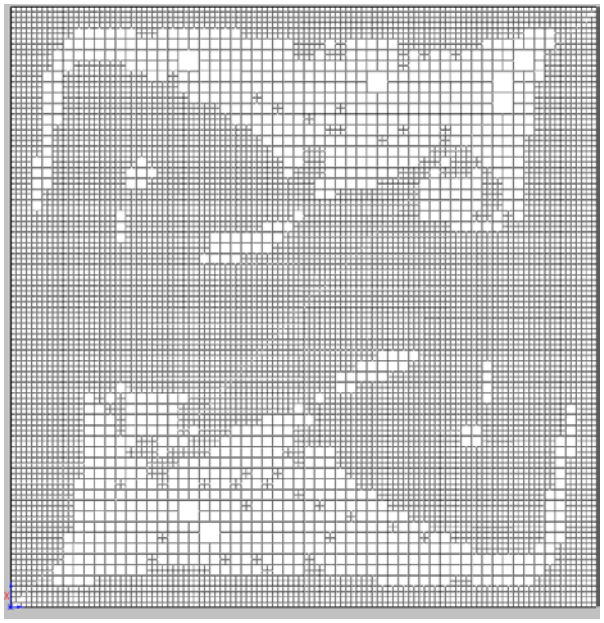

Figure 5. Adapted to the solution mesh at RRL = 8 for $Ra = 10^6$.

The next figures demonstrate a good agreement between EFD.Lab predictions and the benchmark solution both in thermal (see Fig. 6 for the average Nusselt number) and hydrodynamic (see Fig. 7 for the maximum velocity components) fields for all considered values of the Rayleigh number.

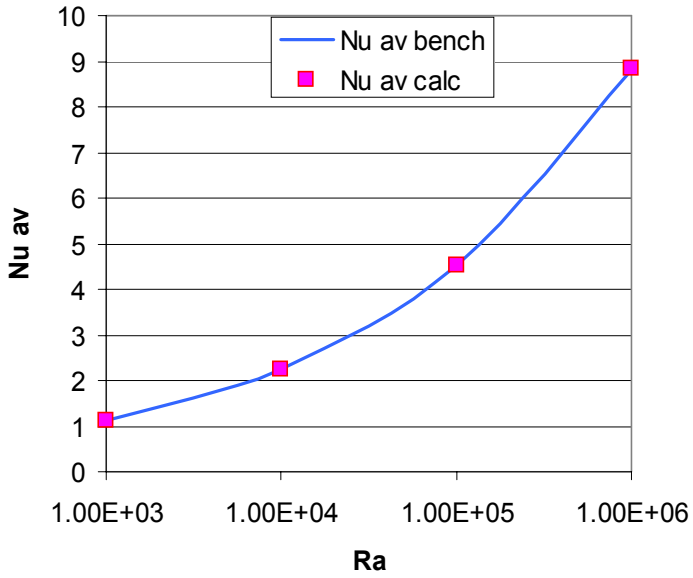

Figure 6. Predicted average Nusselt number vs. Rayleigh number in comparison with the benchmark solution [21].

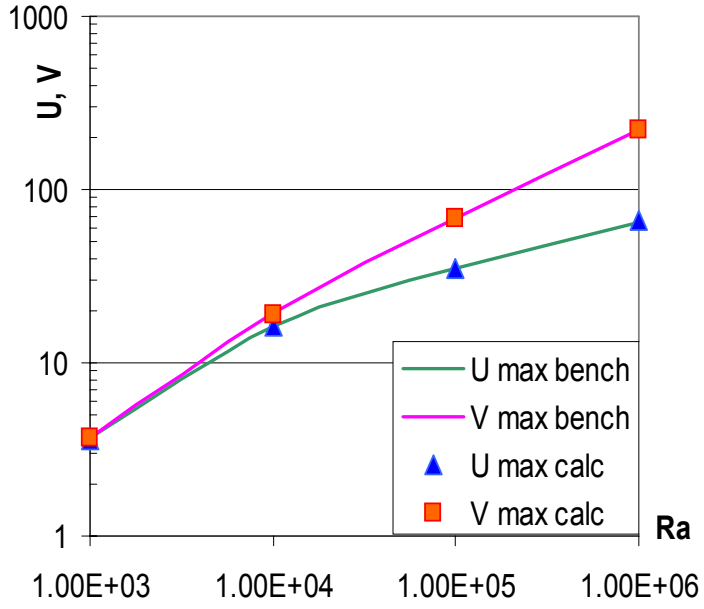

Figure 7. Predicted maximum velocity components vs. Rayleigh number in comparison with the benchmark solution [21].

In the above fundamental tests the V&V procedure were performed separately for various physical effects. Application of EFD.Lab to applied industrial problems with different strongly coupled physical phenomena is presented in the next section.

APPLIED INDUSTRIAL PROBLEMS

The next examples that demonstrate possibility of EFD.Lab to solve problems of practical interest with appropriate accuracy are concerned with electronic cooling.

Nowadays with the increasing of heat dissipation from electronic devices and the reduction of their sizes, thermal management becomes more and more essential element of electronic product design [24]. To increase life and reliability of electronic equipment, it is necessary to preserve its component temperatures within the limits specified by the device design engineers. Heat sinks of various types are the devices constructed to resolve this problem - they enhance heat dissipation from a heat-generating component to air. To optimize performance of a particular heat sink, up-to-date CFD tools are in common use.

Code EFD.Lab demonstrates a very high efficiency and automatic in solving problems of such type. Below there are presented two examples of using EFD.Lab to predict the performance heat sinks at various operating conditions for V&V procedure.

Free convection cooling Performance of a pin-fin heat sink at free convection cooling of air has been studied in [25] both experimentally and numerically using an in-house code. The case of 9x9 square pin-fin array from this work has been investigated via EFD.Lab and compared with measurements.

Our model used in computations (see Fig. 8) totally reproduces the experimental configuration from [25] presented in Fig. 9 in detail. It consists of two rectangular plexiglass enclosures put one inside another. The internal enclosure with aluminium pin-fin array over the heating component flush mounted on the bottom (see Fig. 10) is of actual interest. The external one was employed in experiments only to create natural convection environment. Nevertheless, a half of the whole two-enclosure model (the green domain in Fig. 8) has been used in our predictions in order to reproduce exactly the actual experiments (in contrast to [25] where only the internal enclosure has been considered in calculations).

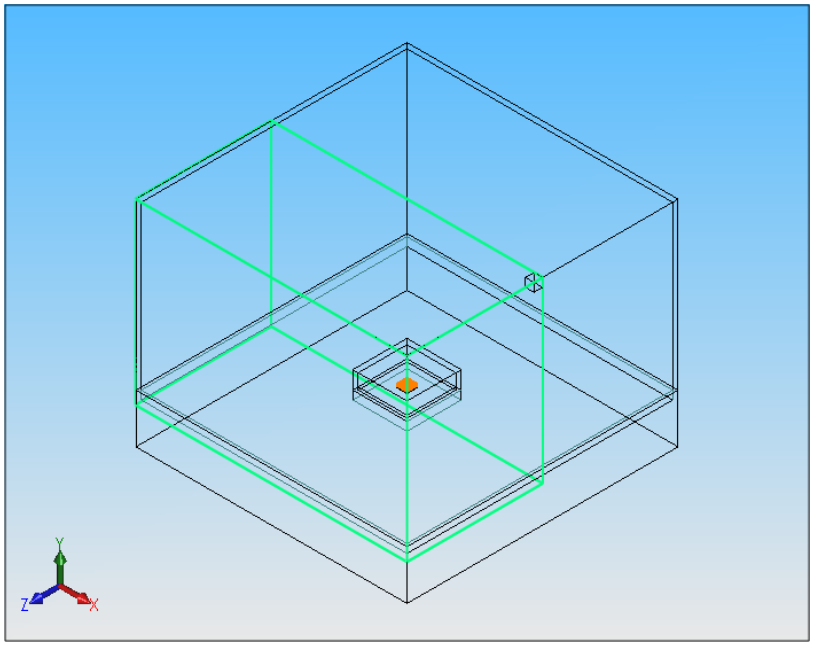

Figure 8. The two-enclosure model with a small box in the wall at the upper corner of the external enclosure for monitoring T_{amb}.

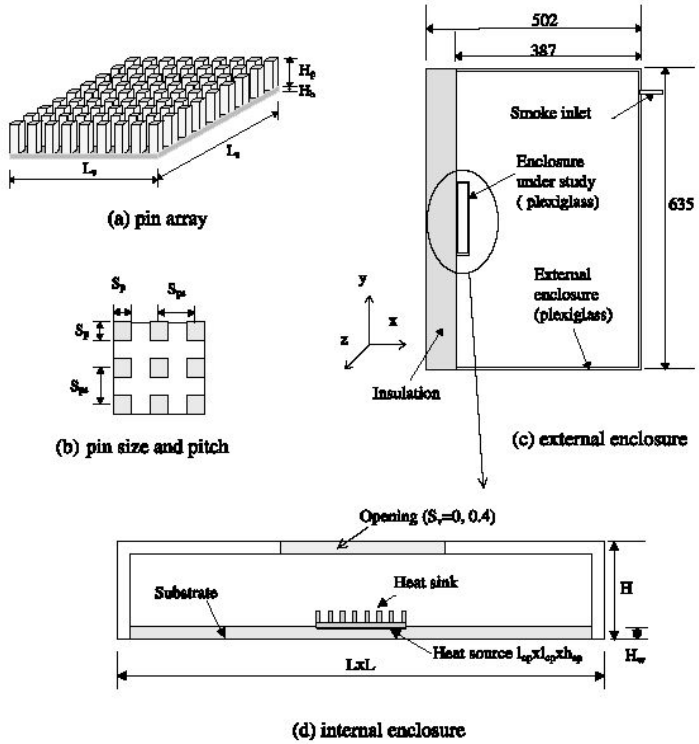

Figure 9. Geometry of enclosures with pin-fin arrays on heating component (from [25]).

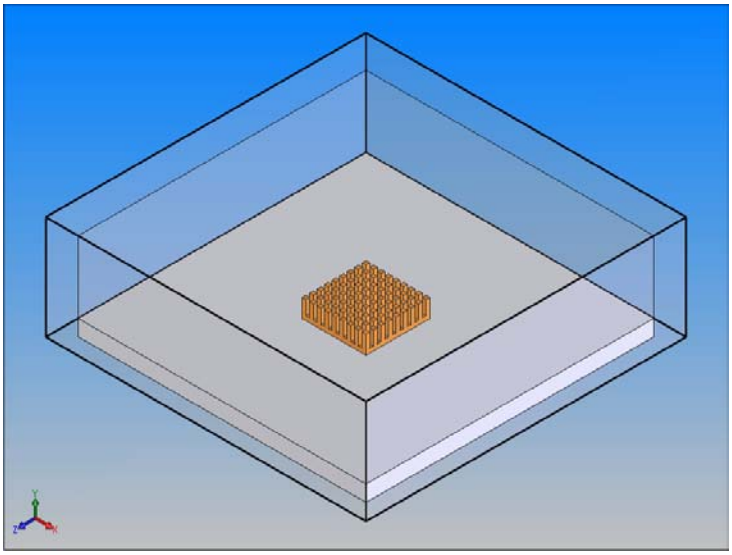

Figure 10. A part of the model: the internal enclosure with 9x9 pin-fin array over the heating component flush mounted on the bottom.

Performance of the pin-fin heat sink has been studied experimentally in [25] at various heat generation rate - q = 0.1, 0.3, 0.5, 0.7 and 1 W – for two configurations of the device – the horizontal case (the gravity force is along y-axis) and the vertical one (the gravity force acts along x-axis of the model).

As it was mentioned above, only the heat sink and heating component are made of aluminium (thermal conductivity k = 200 W/mK), other elements (all walls except for the bottom of the external enclosure) are of plexiglass with k = 0.2 W/mK. The conjugate formulation of the thermal problem in addition to convection and conduction phenomena also includes radiation effects that are essential in this problem (about 50% as it was estimated in [25]). The surface emissivity of the

black painted internal enclosure bottom and pin-fin array was $\varepsilon = 0.95$ and the remaining surfaces of both enclosures are 0.83. The bottom of the external enclosure was made of insulator.

It should be noted that this problem does have some features that make it complicated enough for calculations. First, it has various scales of the model elements: the length of the external enclosure L is 0.635 m, the thickness of the heating component is $\delta = 0.000861$ m and pin fins are of 0.0015x0.0015 m cross-section, i.e. ratio $L/\delta = 737.5$ is very high. It should be mentioned that in computations [25] a porous media model has been used to describe the heat sink in order to simplify essentially the problem geometry. Secondly, heat transfer includes conduction, convection and radiation effects and involves materials with different thermal properties. Next, heat generation rate q is very small – in the range from 0.1 up to 1 W – with the primary searching parameter $R_t=(T_j-T_{amb})/q$. For $q = 0.1$ W the searching temperature drop in R_t is about 5.6 °C that means that for agreement of predictions with measurements within 5 % the temperature field should be predicted with accuracy 0.3 °C. Temperature measurement uncertainty in [25] was estimated as ±0.1 °C that completely satisfies these requirements.

The basic parameter for heat sink efficiency is the thermal resistance between a very thin heating component with prescribed heat generation rate q located under the heat sink and ambient air flow – $R_t=(T_j-T_{amb})/q$ – where T_j is the maximum temperature of the heating component. Namely this parameter was the primary goal of steady-state predictions. As it was mentioned above, a small box in the wall at the upper corner of the external enclosure was employed in EFD.Lab predictions for monitoring T_{amb}.

In spite of the fact that experiments [25] were well-designed in order to minimize the environment impact, inhomogeneous temperature distributions can appear on the outer surfaces of the external enclosure walls due to radiation and convection. To study these effects, three kinds of boundary conditions (except for the insulator) have been considered in EFD.Lab predictions:

- the Newton law of ambient air cooling with convection heat-transfer coefficient h estimated following [20] for the wind-free case. This coefficient depends on the heat generation rate of the component as well as surface position (vertical or horizontal). The values of h were 0.6 and 1.9 W/m^2 K for side walls and the top, respectively, in the case of $q = 0.1$ W. For values of heat generation rate $q = 0.3$-0.7 W values of h were, respectively, 0.73 and 2.3 W/m^2 K, and for $q = 1$ W these are 0.9 and 3 W/m^2 K. A small box in the wall at the upper corner of the external enclosure was employed in EFD.Lab predictions for monitoring T_{amb} (see Fig. 8).
- Isothermal outer wall with specified temperature $T_w = 20$ °C (it is a standard enough value for environment).
- Uniform surface heat sinks of equivalent total rate $-q$ are imposed. This type of the boundary conditions requires no experimental parameters but assumes some distribution of surface sinks (which, in general, may be non-uniform and can be evaluated from preliminary predictions with other boundary conditions).

The initial temperature was $T_{ini} = 20$ °C in all predictions. No-slip, no-permeability conditions for fluid flows were imposed on all internal solid walls.

The whole range of heat generation rate q has been investigated numerically for both configurations of the device. The obtained numerical results are very close to experimental data [25] both for thermal and hydrodynamics parameters and indicate for R_t agreement with measurements within 5% for all considered cases.

Let us consider now the grid convergence study. EFD.Lab essentially exploits adaptive mesh refinement strategy where we have the basic mesh corresponding to the coarser level and successive mesh refinement near boundaries and/or specified objects. The finest grid used in computations has

the basic mesh of 82x52x38 with the total number of cells as high as 375,896 cells (see Figs. 11 (a) and (b), showing various fragments of this mesh along with temperature contours predicted for q = 1 W).

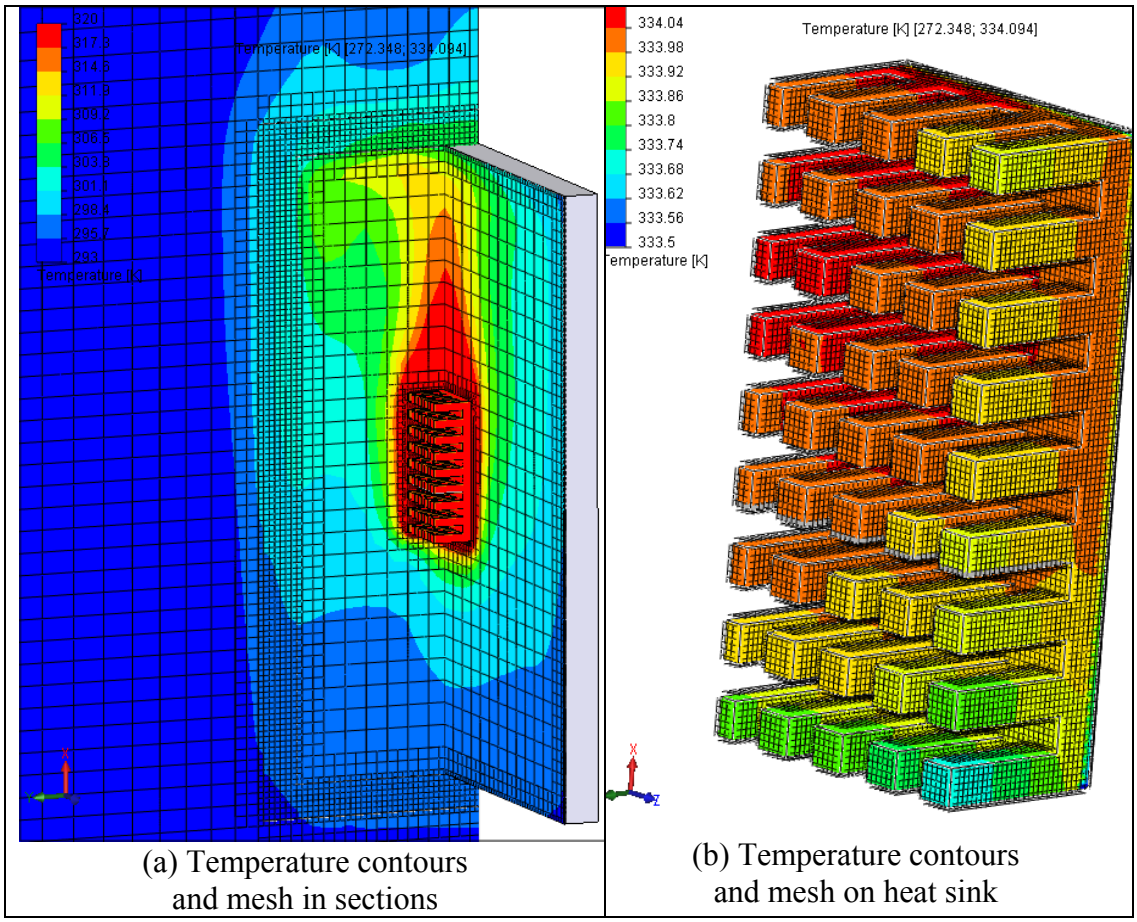

(a) Temperature contours and mesh in sections

(b) Temperature contours and mesh on heat sink

Figure 11. Temperature contours and fragments of the mesh on various surfaces.

So, three grids have been considered for a half of the model with basic meshes of various size with stretching to the external enclosure - 28x18x14 (26,194 cells totally)), 56x35x28 (145,082 cells totally) and 82x52x38 (375,896 cells totally).

Calculations with various boundary conditions have indicated that two types of them - the specified heat-transfer coefficient and imposed uniform surface heat sinks of equivalent total rate $-q$ – provide practically the same numerical results. Predictions with prescribed boundary temperature T_w = 20 °C give the worst results in sense of agreement with experimental R_t . Therefore, all numerical results presented here correspond to the Newton law of ambient air cooling as the most universal for engineering applications type of boundary conditions.

The grid dependence of numerical results on the mesh size is shown in Fig. 12 for two values of q – the minimal and maximal ones - for the vertical configuration of the device. Figure 13 demonstrates a comparison of predicted and measured thermal resistance R_t for different q derived on the finest grid with 375,896 cells. It should be noted again that for all values of q the numerical results are within 5% from experimental data – an excellent correlation between computations and measurements.

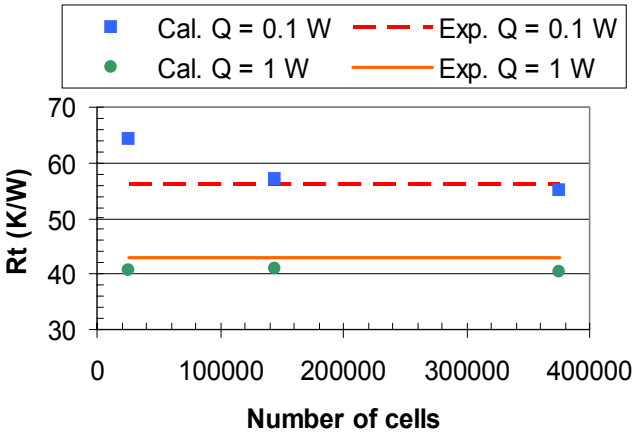

Figure 12. Grid convergence: predicted R_t vs. total cells number, q = 0.1 and 1 W, vertical case.

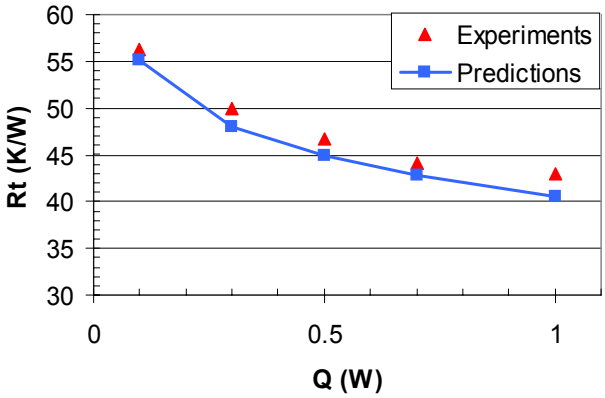

Figure 13. Comparison of predicted and measured thermal resistance R_t for different q, vertical case.

Figure 14 demonstrates flow trajectories colored by the velocity magnitude in both enclosures for the case of q = 1 W. It is easy to see that the flow is fully 3D and so, it is difficult enough to construct computational flow patterns for comparing with the experimental visualization.

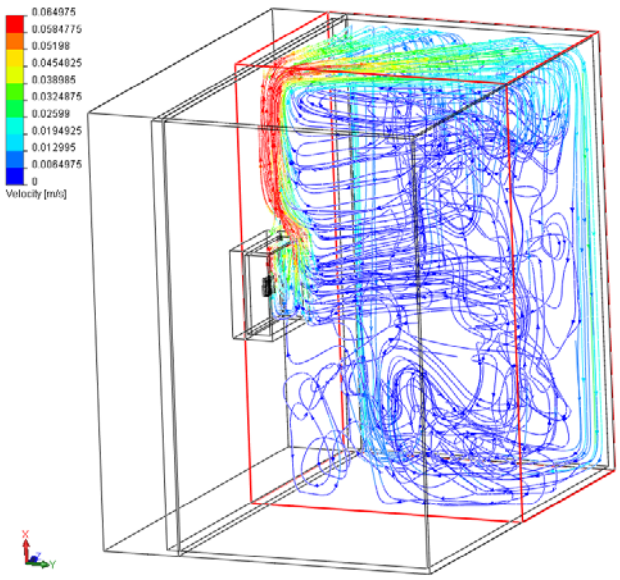

Figure 14. Flow trajectories colored by the velocity magnitude in both enclosures, q = 1 W.

Figure 15 shows a comparison of visualization from [25] with predicted flow pattern for q = 1 W derived on the finest grid. Obviously, a very good agreement is observed here.

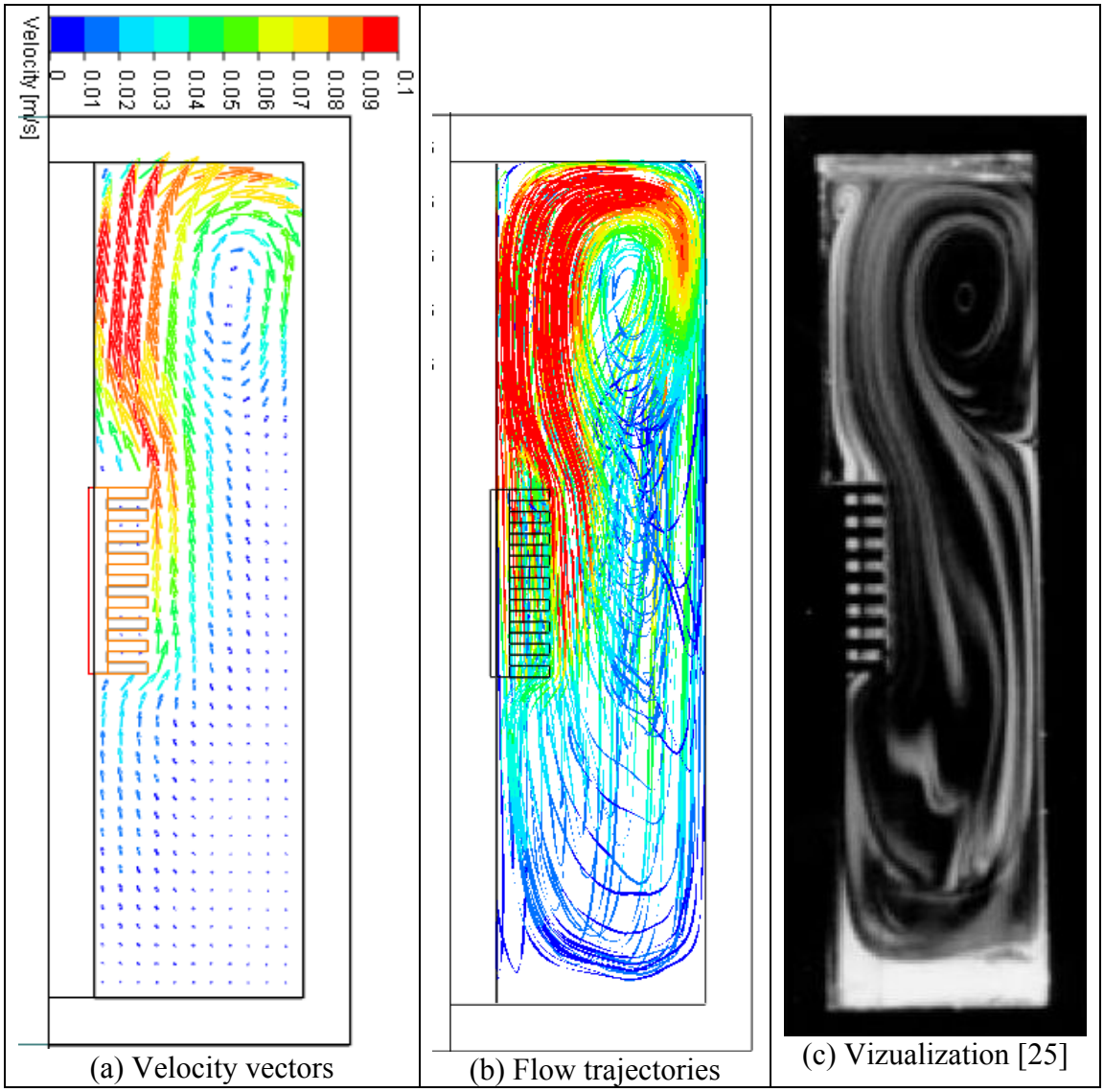

(a) Velocity vectors (b) Flow trajectories (c) Vizualization [25]

Figure 15. Predicted velocity vectors (a) and flow trajectories colored by velocity magnitude (b) in compare with vizualization from [25] (c), q = 1 W, z = 0 m.

A very good coincidence of numerical and experimental results has been obtained for the horizontal configuration of the device, too.

The next figures present a detailed comparison of the predicted flow pattern (see Figs. 16 and 17) with experimental vizualization from [25] (see Fig. 18) for the intermediate value of the heat generation rate q = 0.5 W.

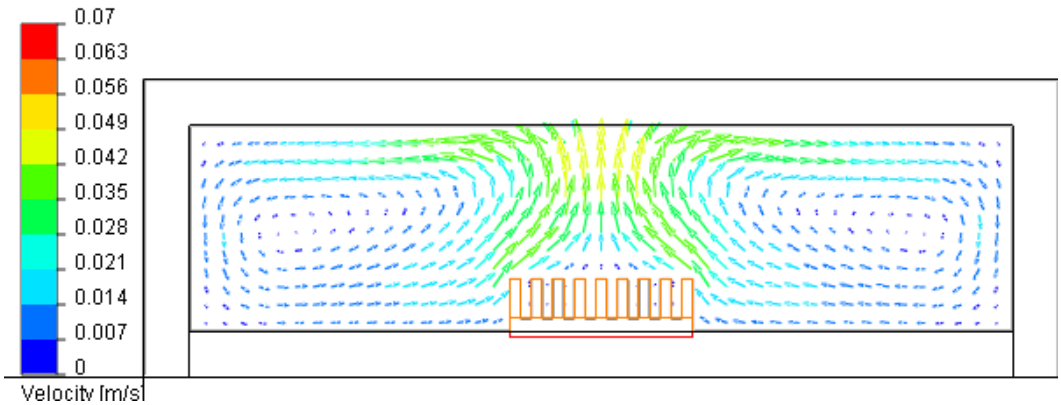

Figure 16. Predicted velocity vectors in the internal enclosure, q = 0.5 W, z = 0 m.

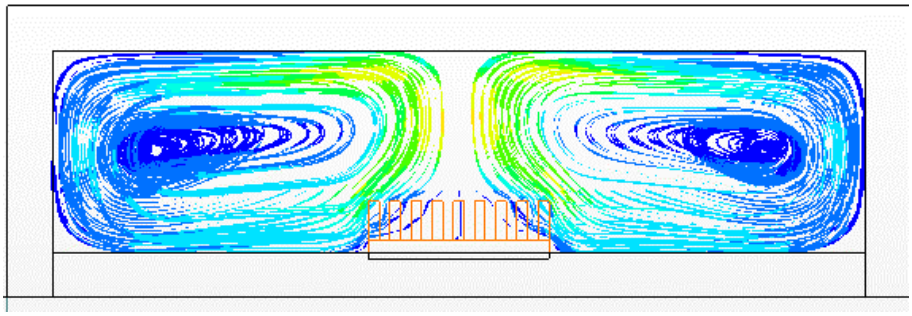

Figure 17. Predicted flow trajectories colored by velocity magnitude, q = 0.5 W.

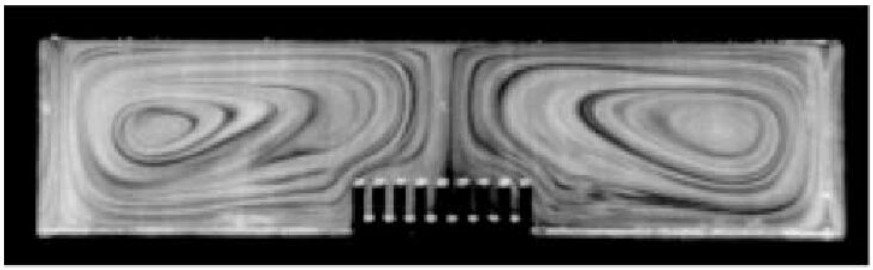

Figure 18. Visualization from [25], q = 0.5 W, z = 0 m.

Increasing of the heat generation rate results in a more intensive flow in both enclosures (see Fig. 19).

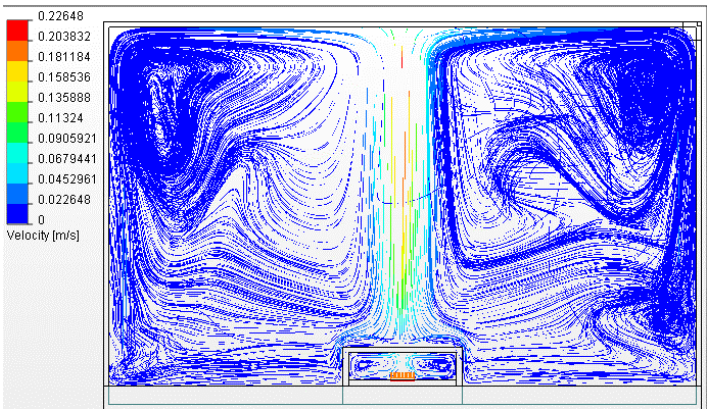

Figure 19. Flow trajectories in both enclosures, q = 1 W.

For this case with q = 1 W a good agreement is also observed between numerical and experimental results presented in Figs. 20, 21 and 22, respectively.

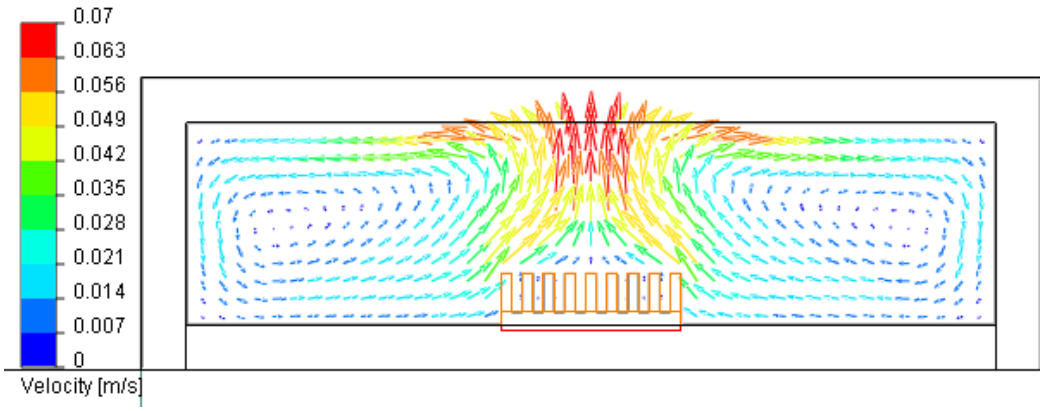

Figure 20. Predicted velocity vectors in the internal enclosure, q = 1 W, z = 0 m.

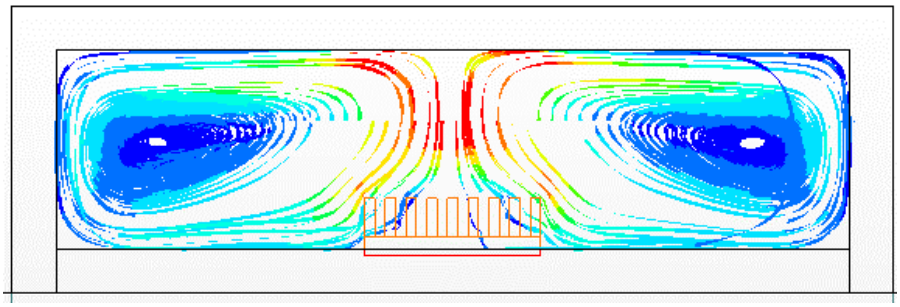

Figure 21. Predicted flow trajectories colored by velocity magnitude, q = 1 W.

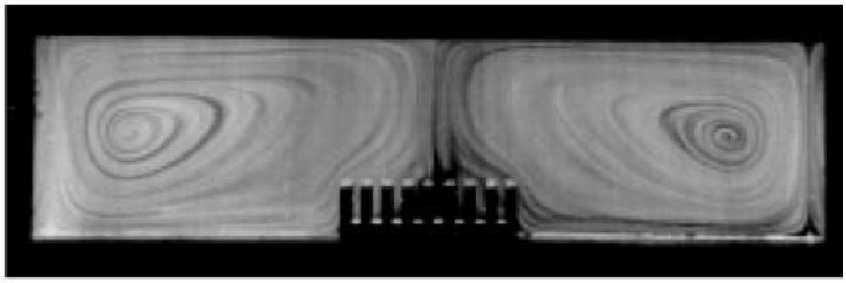

Figure 22. Visualization from [25], q = 1 W, z = 0 m.

Forced convection cooling Another type of heat sinks – plane ones – has been also studied numerically using EFD.Lab. Wind tunnel experimental results from [26] have been used for validation and verification of EFD.Lab predictions of forced air cooling in a duct. The most complicated case with the dense heat sink (32 plates) and large clearance (30% in all directions) has been considered.

The duct of rectangular cross-section has a heating component flush mounted on the bottom with plain heat sink of 32 plates located over it (see Fig. 23). Internal sizes of the duct are L = 0.61 m, W = 0.0923 m and H = 0.0663 m. All its walls are made of FR-4 (fiberglass-epoxy laminate board with thermal conductivity k = 0.35 W/mK) with thickness δ = 0.005 m. A fan provides a uniform velocity profile of air with T_{amb} = 25 °C at the duct inlet. The opening with the atmospheric pressure is at the duct outlet. The heating component (k = 220 W/mK) with L = 0.11 m, W = 0.071 m and H

= 0.0005 m is located at the distance of 0.17 m from the inlet with the heat generation rate 100 W. To enhance heat transfer from it, the heat sink is attached to the top. It consists of the aluminium base (k = 220 W/mK) with height H = 0.005 m and 32 plates (k = 150 W/mK) with H = 0.045 m and W = 0.0005 m located in a duct in the side-inlet-side-exit (SISE) configuration with respect to an incoming air flow (see Fig. 24).

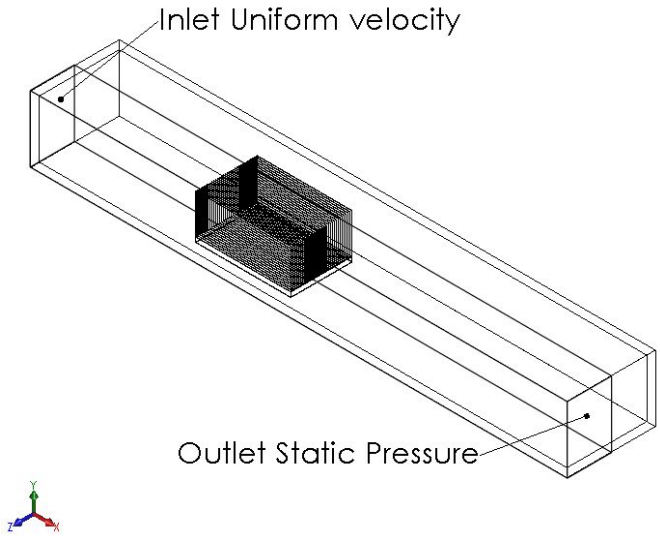

Figure 23. The computational model.

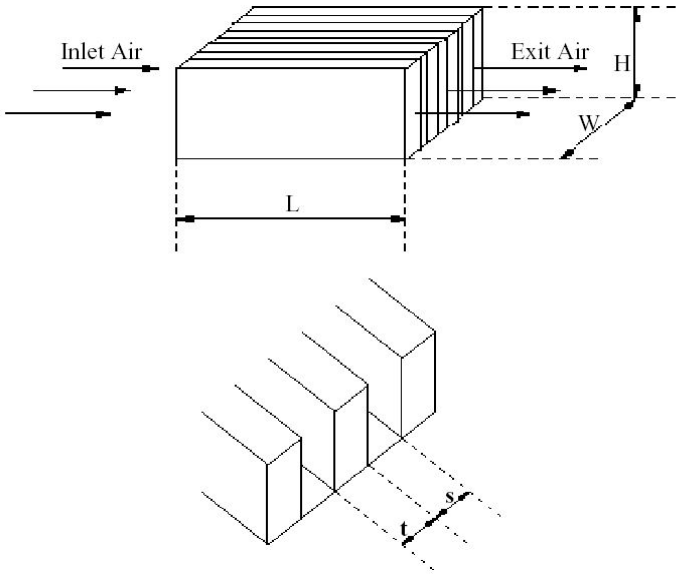

Figure 24. SISE-configuration of plain heat sinks (from [26]).

Steady-state heat and fluid flows have been calculated in a half of the model for two values of the inlet velocity u, namely, 3 and 5 m/s. Radiation between the heat sink (emissivity ε = 0.9) and duct walls (ε = 0.9) was taken into account in addition to convection and conduction. At the outer surfaces of all walls (except for the thermally-insulated bottom) there is imposed the Newton law of ambient air cooling with convection heat-transfer coefficient $h = 5.6 + 4*u$ (W/m^2 K), taken from [27] for the wind case, where u is the inlet velocity, supplemented with radiation into the non-radiative environment.

In addition to measurements some numerical results obtained via code IcePak developed by FLUENT Inc. are presented in work [26]. It is not clarified clearly in this work are radiation effects essential or not in this problem at the considered regimes. Estimated Reynolds numbers are low enough for the considered flow regimes. Predictions via code IcePak have been conducted in two regimes – laminar and turbulent – and indicated different agreement with measurements, namely, 7% error in laminar and 15-20% error in turbulent predictions, respectively (grid was between 110,000 and 210,000 elements). EFD.Lab predictions have been carried out in the laminar regime because local Reynolds number for the flow between plates is lower 500 for all inlet velocities. Calculations have indicated that omitting radiation results in overprediction of the thermal resistance on about 10%. Only taking into account the radiative fluxes from all surfaces it is possible to obtain numerical results maximally close to measurements.

For the grid convergence study three grids have been considered for a half of the model with basic meshes of various size - 30x11x17 (90,107 cells totally), 45x16x22 (203,972 cells totally) and 68x24x24 (456,872 cells totally). The grid convergence of the solution for u = 3 and 5 m/s is presented in Fig. 25. Figure 26 demonstrates a comparison of predicted and measured thermal resistance R_t for different u obtained on the finest grid with 456,872 cells. Agreement between numerical results and measurement data was within 5% for both velocity values - a very good result again.

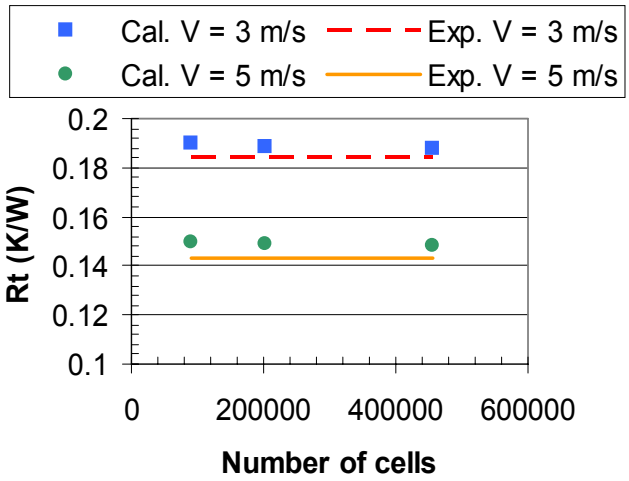

Figure 25. Grid convergence: predicted R_t vs. total cells number for u = 3 and 5 m/s.

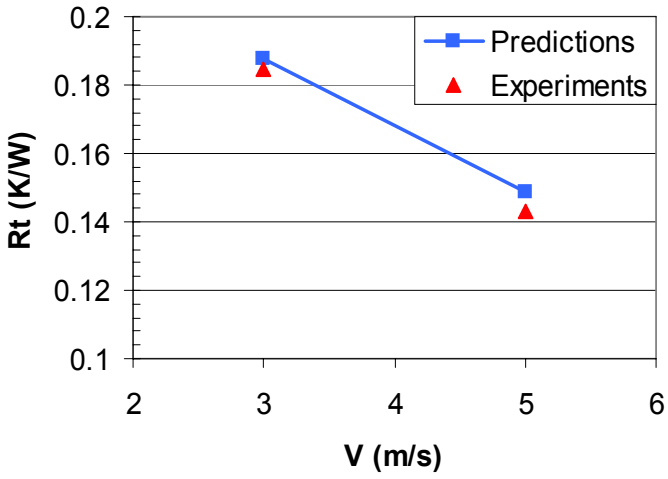

Figure 26. Comparison of predicted and measured thermal resistance R_t for different u.

Predicted flow trajectories and the temperature field are shown for u = 5 m/s in Figs. 27 and 28, respectively. Contours of the temperature and velocity module in transverse cross-section x = 0.25 m are presented in Fig. 29.

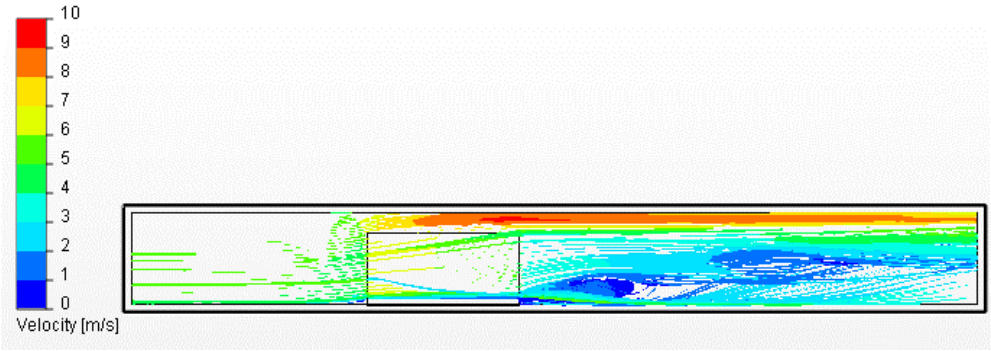

Figure 27. Flow trajectories (colored by velocity magnitude) in the duct, u = 5 m/s.

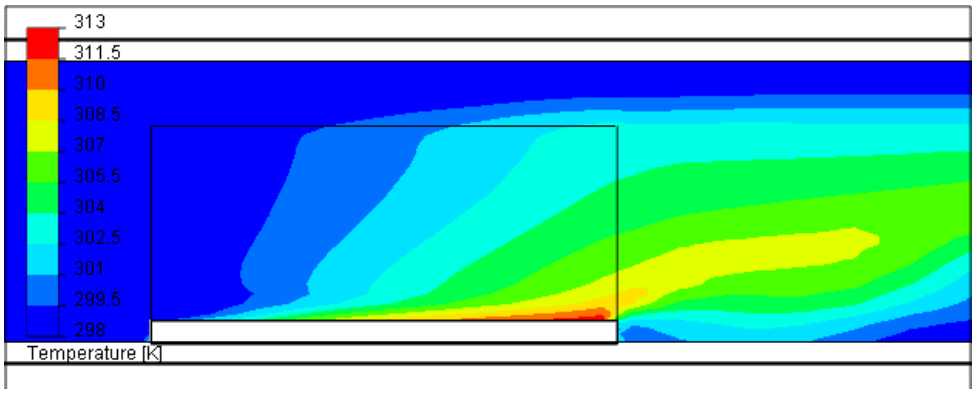

Figure 28. Temperature contours in the vicinity of plane sink, u = 5 m/s, z = 0 m.

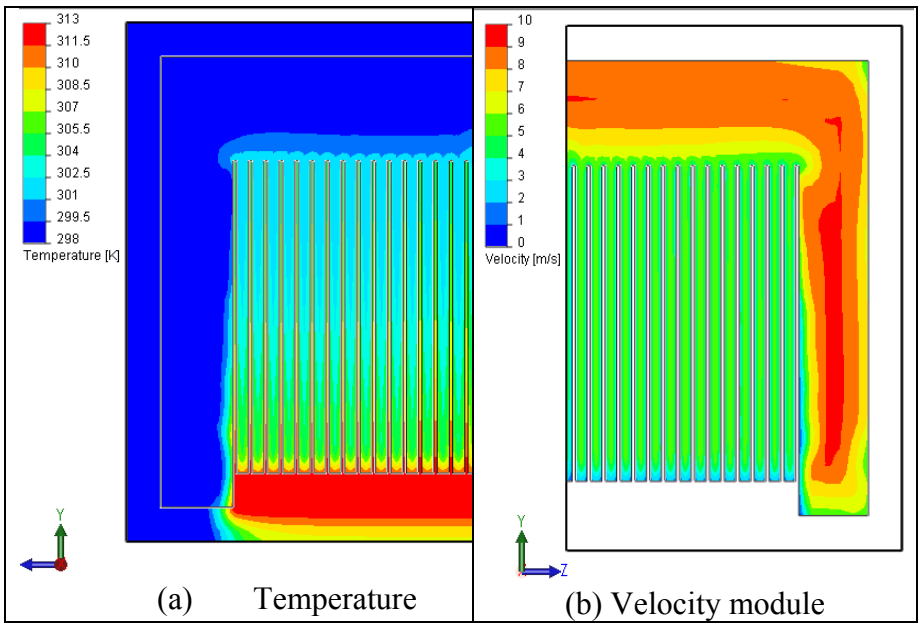

Figure 29. Contours of the temperature (a) and velocity module (b), u = 5 m/s, x = 0.25 m.

Figure 30 demonstrates contours of the temperature and the adaptive computational grid with 456,872 cells in longitudinal (z = 0 m) and transverse (x = 0.225 m) cross-sections, respectively.

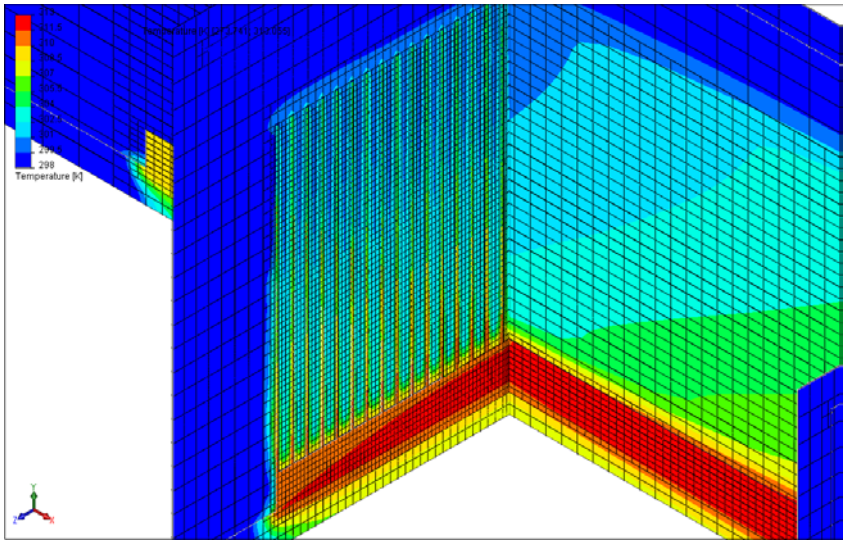

Figure 30. Contours of the temperature and the adaptive grid in cross-sections z = 0 m and x = 0.225 m, u = 5 m/s.

To show efficiency of the solver, the total computation time divided by the total number of cells and by the number of iterations is depicted in Fig. 31 for both above problems. These data correspond the vertical configuration with q = 1 W for the pin-fin sink and u = 5 m/s for the plane heat sink. It should be noted that the number of iterations was the same for all computational grids and equaled 400 for the pin-fin sink problem and 150 for the forced convection cooling. Evidently, the solver used for solving grid equations at each iteration, indicates the number of arithmetic operations proportional to the number of grid points (cells). All runs have been performed using PC with a processor of 2.8 Ghz. Runs on appropriate in sense of accuracy grids required about 4 hours on the grid with 145,082 cells for the pin-fin sink problem and about 2.7 hours on the grid with 203,972 cells for the plane heat sink – it is a good result for such a class of heat and fluid flow problems.

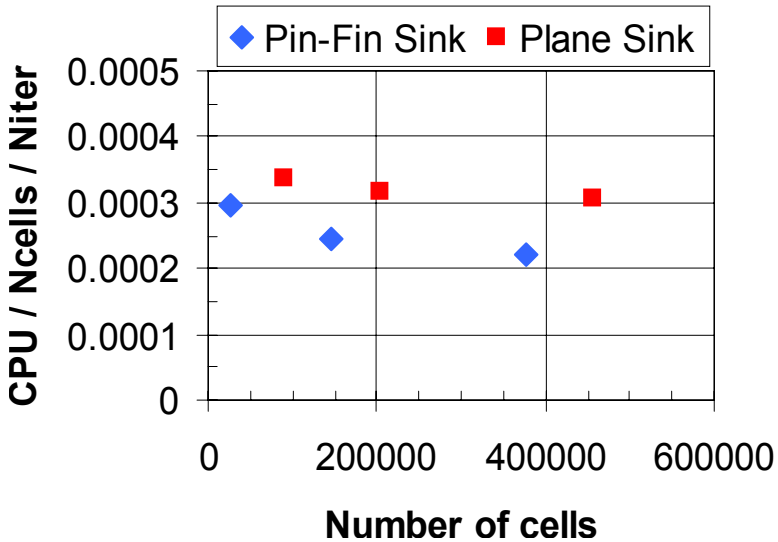

Figure 31. CPU time per cell per iteration vs. number of cells.

CONCLUSION

As the rule, practically any attempt to reproduce experimental results for an applied industrial problem faces the necessity to reconstruct absent input data via human imagination. This is especially true with respect to thermal problems because heat transfer phenomenon is coupled with various effects (radiation, variation in material properties *etc*.) and their impact on experimental and/or numerical results is unknown a priori. So, experiments with complete and sufficiently accurate data for all input parameters are necessary. Measurements from [25] are a good example of such a well-designed experimental work.

A very good agreement has been obtained between numerical and experimental data in all presented here examples of EFD.Lab predictions. Needless to say that this collection should be and will be more and more wide. But even now it is obvious that EFD.Lab can serve as an efficient tool to study engineering problems including the heat transfer phenomenon.

Notwithstanding a lot of databases with complicated CFD tests, fundamental tests continue to provide an essential part of the V&V-procedure due to their low cost in time and the possibility to study on a single model a wide range of heat and flow regimes and effects.

REFERENCES

1. Elliot, L., CFD Applications Soar: Part Two, *CFD Review,* June 11, 2003 (http://www.cfdreview.com/articles/).
2. Freitas, C.J., Perspective: Selected Benchmarks From Commercial CFD Codes, *Trans. ASME, J. Fluids Engrg.*, Vol. 117, No. 2, pp 208-218, 1995.
3. Fluid Dynamics Databases, *ERCOFTAC Bulletin,* No. 52, 2002.
4. Berger, M.J. and Oliger, J., Adaptive Mesh Refinement for Hyperbolic Partial Differential Equations, *J. Comput. Phys.*, Vol. 53, No. 3, pp 482-512, 1984.
5. Berger, M.J. and Colella, P., Local Adaptive Mesh Refinement for Shock Hydrodynamics, *J. Comput. Phys.*, Vol. 82, No. 1, pp 64-84, 1989.
6. Gavrilyuk, V.N., Denisov, O.P, Nakonechny, V.P., Odintsov, E.V., Sergienko, A.A. and Sobachkin, A.A., Numerical Simulation of Working Processes in Rocket Engine Combustion Chamber, *44th Congress of the Int. Astronautical Federation*, Graz, Austria, October 16-22, 1993, IAF-93-S.2.463, pp 1-15.
7. Krulle, G., Gavriliouk, V., Schley, C.-A. and Sobachkin, A., Numerical Simulation Technology of Aerodynamic Processes and Its Applications in Rocket Engine Problems, *45th Congress of the Int. Astronautical Federation*, Jerusalem, Israel, October 9-14, 1994, IAF-94-S2.414, pp 1-12.
8. Hagemann, G., Schley, C.-A., Odintsov, E and Sobatchkine, A., Nozzle Flowfield Analysis with Particular Regard to 3D-Plug-Claster Configurations, *32nd AIAA/ASME/SAE/ASEE Joint Propulsion Conf.*, Lake Buena Vista, FL, July 1-3, 1996, AIAA-96-2954, pp 1-16.
9. Schley, C.-A., Deplanque, J., Merkle, C., Duthoit, V. and Gavriliouk, V., Fundamental and Technological Aspects of Combustion Chamber Modeling, *Proc. 3rd Int. Symp. Space Propulsion,* Beijing, China, August 11-13, 1997, pp 1-15.
10. Pavlov A.N., Sazhin, S.S., Fedorenko, R.P. and Heikal, M.R., A Conservative Finite Difference Method and Its Application for Analysis of a Transient Flow around a Square Prizm, *Int. J. Numer. Methods Heat Fluid Flow,* Vol. 10, No. 1, pp 6-46, 2000.

11. Fedorenko, R.P., A Relaxation Method for Solving Elliptic Difference Equations, *Z. Vychisl. Mat. Mat. Fiz.,* Vol. 1, No. 5, pp 922-927 (= *USSR Comp. Math. Math. Phys.*, Vol. 1, pp 1092-1096, 1961).
12. Trottenberg, U., Oosterlee, C.W., Schuller, A. with Brandt, A., Oswald, P. and Stuben. K., *Multigrid,* Academic Press, San Diego, 2001.
13. Roache, P.J., *Verification and Validation in Computational Science and Engineering,* Hermosa, Albuquerque, NM, 1998.
14. Stern, F., Wilson, R.V., Coleman, H.W. and Paterson, E.G., Verification and Validation of CFD Simulations, *IIHR Report No. 407,* Iowa Inst. Hydraulic Research, the University of Iowa, 1999.
15. Oberkampf, W.L. and Trucano, T.G., Verification and Validation in Computational Fluid Dynamics, *Progress in Aerospace Sciences,* Vol. 38, pp 209-272, 2002.
16. Van Dyke, M., *An Album of Fluid Motion*, The Parabolic Press, Stanford, CA, 1982.
17. Panton, R.L., *Incompressible Flow,* 2nd ed., Wiley, New York, 1996.
18. Zdravkovich, M.M, *Flow Around Circular Cylinders, Vol. 1: Fundamentals*, Oxford University Press, New York, 1997.
19. Zdravkovich, M.M, *Flow Around Circular Cylinders, Vol. 2: Applications*, Oxford University Press, New York, 2003.
20. Holman, J.P., *Heat Transfer,* 8th ed., McGraw-Hill, New York, 1997.
21. Davis, G. de Vahl, Natural Convection of Air in a Square Cavity: a Bench Mark Numerical Solution, *Int. J. Numer. Methods Fluids*, Vol. 3, No. 3, pp 249-264, 1983.
22. Emery, A. and Chu, T.Y., Heat Transfer across Vertical Layers, *Trans. ASME, J. Heat Transfer*, Vol. 87, p 110, 1965.
23. Pepper, D.W and Hollands, K.G.T., Benchmark Summary of Numerical Studies: 3-D Natural Convection in an Air-Filled Enclosure, *CHT'01: Advances in Computational Heat Transfer II* (Eds. G. de Vahl Davis and E. Leonardi), Vol. 2, pp 1323-1329, Begell House Inc., New York, 2001.
24. Lee, S., How to Select a Heat Sink, *Cooling Zone*, June, 2001 (http://www.coolingzone.com/Content/Library/Papers/index.html#Design).
25. Yu, E. and Joshi, Y., Heat Transfer Enhancement from Enclosed Discrete Components Using Pin-Fin Heat Sinks, *Int. J. Heat Mass Transfer*, Vol. 45, No. 25, pp 4957-4966, 2002.
26. Prstic, S., Iyengar, M. and Bar-Cohen, A., Bypass Effect in High Performance Heat Sinks, *Proc. Int. Thermal Sciences Conf.*, Bled, Slovenia, June 11-14, 2000, pp 1-8.
27. Kuchling, H., *Physik,* VEB FachbuchVerlag, Leipzig, 1980.